

Article

Counter Anion Effects on the Formation and Structural Transformations of Mo(VI)-Hydrazone Coordination Assemblies: Salts, Solvates, Co-Crystals, and Neutral Complexes

Mirna Mandarić¹, Biserka Prugovečki¹, Ivana Kekez¹, Danijela Musija², Jelena Parlov Vuković³, Marina Cindrić¹ and Višnja Vrdoljak^{1,*} 

¹ Department of Chemistry, Faculty of Science, University of Zagreb, Horvatovac 102a, 10000 Zagreb, Croatia; mirna.mandacic@chem.pmf.hr (M.M.); biserka@chem.pmf.hr (B.P.); ikekez@chem.pmf.hr (I.K.); marina@chem.pmf.hr (M.C.)

² Department of Chemistry and Biochemistry, School of Medicine, University of Zagreb, Šalata 3, 10000 Zagreb, Croatia; danijela.musija@mef.hr

³ Product Development Department, Refining & Marketing Business Division, INA-Industrija Nafta d.d., Lovinčičeva bb, 10002 Zagreb, Croatia; jelena.parlov-vukovic@ina.hr

* Correspondence: visnja.vrdoljak@chem.pmf.hr; Tel.: +385-1-4606-353



Citation: Mandarić, M.; Prugovečki, B.; Kekez, I.; Musija, D.; Parlov Vuković, J.; Cindrić, M.; Vrdoljak, V. Counter Anion Effects on the Formation and Structural Transformations of Mo(VI)-Hydrazone Coordination Assemblies: Salts, Solvates, Co-Crystals, and Neutral Complexes. *Crystals* **2022**, *12*, 443. <https://doi.org/10.3390/cryst12040443>

Academic Editor:
Ana M. Garcia-Deibe

Received: 5 March 2022

Accepted: 18 March 2022

Published: 22 March 2022

Publisher's Note: MDPI stays neutral with regard to jurisdictional claims in published maps and institutional affiliations.



Copyright: © 2022 by the authors. Licensee MDPI, Basel, Switzerland. This article is an open access article distributed under the terms and conditions of the Creative Commons Attribution (CC BY) license (<https://creativecommons.org/licenses/by/4.0/>).

Abstract: Complex salts [1H]X and [1H](XA)_{0.5}·2MeOH, and co-crystals [1H]X·0.5VA (X = chloride or bromide, XA = chloranilate or bromanilate, VA = *o*-vanillin azine), comprising [MoO₂(HL)(MeOH)]⁺ ([1H]⁺) cation (H₂L = 3-methoxysalicylaldehyde isonicotinoyl hydrazone), were prepared either by solution-based synthesis or by mechanochemical synthesis. Whereas [1H]X salts were extremely sensitive to humidity, their stability could be reinforced by the azine incorporation into the complex network. Solvent-mediated transformations of [1H]X led to methanol co-ligand replacement and afforded complexes [MoO₂(HL)X] (2Cl·MeOH, 2Cl, and 2Br·0.5MeCN). However, solvates [1H](XA)_{0.5}·2MeOH, under the same conditions, gave stable complexes [1H](XA)_{0.5} in which methanol remained coordinated. The differences in the assembly's behavior were attributed to the packing arrangements, the relative orientation of cations and anions, and interactions between them. Polymorph [MoO₂(L)(MeOH)] (1), not attainable by other routes, was the only product when compounds [MoO₂(HL)X] were treated with a weak base at low temperatures. Tetranuclear [MoO₂(L)]₄ and polynuclear [MoO₂(L)]_n (2) supramolecular isomers, concomitantly crystallized when the reaction was conducted solvothermally. All of the complexes were characterized using X-ray diffraction methods (SCXRD and PXRD), spectroscopic methods (ATR-IR and solution-state and solid-state MAS NMR), and elemental and thermal analyses. The cytotoxicity of the different types of compounds against THP-1 and HepG2 cells was also evaluated.

Keywords: molybdenum; hydrazone; solvates; complex salts; co-crystals; coordination polymer; chloranilate; *o*-vanillin azine

1. Introduction

Aroylhydrazones R¹R²C=N–NH–(C=O)R³ represent an important class of compounds in the design and synthesis of supramolecular and coordination assemblies [1]. They are very versatile ligands possessing several potential donor sites for metal coordination [2–7]. Hydrazones can act as neutral or anionic ligands and link metal ions via different coordinative modes, thus forming metal complexes having attractive structures, from discrete to extended ones, featuring one-, two-, and three-dimensional motifs [1].

One of the significant features of hydrazones is the ability to adjust their properties via steric and electronic effects of aldehyde and hydrazide components [8]. In this context, the chemistry of metallosupramolecular Mo-hydrazones has also become the subject of much

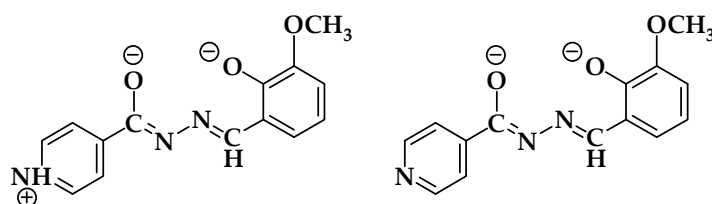
interest over the last decade [9–11]. A number of coordination compounds with interesting structures, and biological or catalytic properties, have been studied [12–20].

An introduction of additional organic and inorganic units enables a way to create multi-component networks, salts, solvates, or co-crystals, having even greater structural diversity [21,22], and provides a chance to modify the existing properties of such materials [23]. Their formation greatly relies on non-covalent interactions such as hydrogen bonds, halogen bonds, and π -stacking. However, little attention has been given to Mo-hydrazone multi-component species. A rare example of the structurally characterized complex is $[\text{MoO}_2(\text{C}_{14}\text{H}_9\text{ClN}_2\text{O}_4)(\text{CH}_3\text{OH})]\cdot\text{C}_{10}\text{H}_8\text{N}_2$ co-crystallized with 4,4'-bipyridine [24]. Furthermore, salts of Mo(VI) complexes with tridentate hydrazone ligands are also rare. Only a few protonated complexes with inorganic counter anions have been reported [25–27].

Anilic acids can be used as interesting building blocks for supramolecular architectures [28–33]. They can undergo multistep deprotonation processes, thus offering possibilities of different aggregations between the building units as found in $[\text{Fe}(\text{Hpbph})_2](\text{ClA})\cdot 2\text{CH}_3\text{OH}$, $[\text{Fe}(\text{Hpbph})_2](\text{HClA})_2\cdot 2\text{THF}$, and $[\text{Fe}(\text{Hpbph})_2](\text{ClA})(\text{H}_2\text{ClA})_2\cdot 2\text{CH}_3\text{CN}$ (Hpbph = 2-(diphenylphosphino)benzaldehyde-2-pyridylhydrazone, H_2ClA = chloranilic acid) [34]. Interestingly, Pd(II)-hydrazone complex $[\text{PdBr}(\text{Hmtbhp})]_2(\text{HBrA})_2(\text{H}_2\text{BrA})\cdot 2\text{CH}_3\text{CN}$ (Hmtbhp = 2-(2-(2-(methylthio)benzylidene)hydrazinyl)pyridine, H_2BrA bromanilic acid), exhibits vapochromic behavior depending on the proton-donating ability of the solvent vapor molecules [35]. Nevertheless, they may act as bridging (bis)bidentate or terminal bidentate ligands [36–38].

Similarly, azines $\text{R}^1\text{R}^2\text{C}=\text{N}-\text{N}=\text{CR}^3\text{R}^4$, i.e., N–N linked diimines, are well known to serve as polydentate ligands in metal complexes, or act as bridging ligands through nitrogen atoms [39,40]. But they can also participate in hydrogen bond-directed and π -stacking-directed packing [41]. In such a way they can be associated with coordination compounds to give new supramolecular architectures. A rare example of such Mo(VI) azine multi-component complex is $[\text{Mo}_2\text{O}_4(\mu_2\text{-O})(\text{H}_2\text{O})_2(\text{L})]_2\cdot\text{L}\cdot\text{L}\cdot\text{L}\cdot\text{L}\cdot[\text{Mo}_2\text{O}_4(\mu_2\text{-O})(\text{H}_2\text{O})_2(\text{L})]_2$ (L = 6,6'-(1*E*,1'*E*)-hydrazine-1,2-diylidenebis(methanelylidene))bis(3-(diethylamino))phenol) [42].

Considering the mentioned aspects, in this work we aimed to investigate (i) the effect of the reaction conditions on the formation of the complex salts $[\text{MoO}_2(\text{HL})(\text{MeOH})]\text{X}$ (H_2L = 3-methoxysalicylaldehyde isonicotinoyl hydrazone ligand, Scheme 1, $\text{X}^- = \text{Cl}^-$ and Br^-), (ii) the properties of charged complexes in the presence of competing anions/ligands (derived from chloranilic acid or bromanilic acid, and *o*-vanillin azine), (iii) the propensity of complex salts to yield multicomponent assemblies driven by non-covalent interactions, (iv) counter anion effects on structural transformation of complex salts under mild conditions, and (v) influence of reaction conditions on the formation of the deprotonated Mo-hydrazone complexes. We also evaluated the cytotoxicity of the different types of compounds obtained.



Scheme 1. A schematic presentation of 3-methoxysalicylaldehyde isonicotinoyl hydrazone ligand, singly-deprotonated (HL^-), and doubly-deprotonated (L^{2-}) ligand forms.

The products were characterized by single-crystal and powder X-ray diffraction methods (SCXRD, PXRD), solution and solid-state NMR, ATR-IR, as well as thermal analysis (TG). The main intermolecular interactions were identified and analyzed to establish the factors responsible for salt/co-crystal formation. Their stability was correlated with the protonation state of the components and crystal packing features.

2. Materials and Methods

2.1. Synthesis

[MoO₂(acac)₂] [43], [MoO₂Br₂(dmf)₂] [44], [MoO₂Cl₂] [45], 3-methoxysalicylaldehyde isonicotinoyl hydrazone (H₂L) [46], and *o*-vanillin azine (VA) [47] were prepared according to the published procedures. Methanol was dried by the use of magnesium and iodine and then distilled. Dichloromethane and acetonitrile were dried by the use of phosphorus pentoxide and then distilled. Chloranilic acid (H₂ClA) and bromanilic acid (H₂BrA) were purchased from Alfa Aesar (Lancashire, UK). All other chemicals were purchased from Aldrich (Amsterdam, The Netherlands) and used without purification. Elemental analyses were acquired by the Analytical Services Laboratory of the Ruđer Bošković Institute, Zagreb. All analytical data are given in the Supplementary Materials.

2.1.1. Synthesis of [MoO₂(HL)(MeOH)]Cl·MeOH ([1H]Cl·MeOH)

[MoO₂Cl₂] (0.12 g, 0.60 mmol) was added to a solution of H₂L (0.17 g, 0.60 mmol) in 50 mL of dry methanol in a quartz flask. The reaction mixture was irradiated with UV light of 254 nm for two hours and then left at room temperature. After five days, orange crystals were filtered and dried in a desiccator at −15 °C. Yield: 101 mg, 33.6%.

2.1.2. Synthesis of [MoO₂(HL)(MeOH)]Br ([1H]Br)

[MoO₂Br₂(dmf)₂] (0.26 g, 0.60 mmol) was added to the solution of H₂L (0.17 g, 0.60 mmol) in 50 mL of dry methanol. The reaction mixture was left at room temperature overnight. The solution was evaporated to one-half of its volume. The obtained orange precipitate was filtered and dried in a desiccator at −15 °C. Yield: 180 mg, 58.8%.

2.1.3. Synthesis of [MoO₂(HL)(MeOH)](ClA)_{0.5}·2MeOH ([1H](ClA)_{0.5}·2MeOH)

[MoO₂Br₂(dmf)₂] (0.1302 g, 0.30 mmol) was added to a solution of chloranilic acid (0.0940 g; 0.45 mmol) in 20 mL of dry methanol, and the reaction mixture was left at room temperature for a few hours. H₂L (0.0814 g, 0.30 mmol) was added to the resulting solution. After several days copper-red coloured crystals appeared. The crystalline product [1H](ClA)_{0.5}·2MeOH was filtered and washed using a small amount of cold methanol. The crystals were quickly transferred on a dry filter paper into a desiccator and then placed in a freezer (at −15 °C). Yield: 45 mg, 28.1%.

2.1.4. Synthesis of [MoO₂(HL)(MeOH)](BrA)_{0.5}·2MeOH ([1H](BrA)_{0.5}·2MeOH)

[MoO₂Br₂(dmf)₂] (0.1302 g, 0.30 mmol) was added to a solution of bromanilic acid (0.1341 g, 0.45 mmol) in 20 mL of dry methanol, and the reaction mixture was left at room temperature for a few hours. H₂L (0.0814 g, 0.30 mmol) was added to the resulting solution. After several days reddish-brown coloured crystals of [1H](BrA)_{0.5}·2MeOH appeared. The product was filtered, washed using a small amount of cold methanol, and dried in a desiccator up to a constant weight (at −15 °C). Yield: 25 mg, 13.0%.

2.1.5. Synthesis of [MoO₂(HL)(MeOH)]Cl·0.5VA ([1H]Cl·0.5VA)

Method A. The solid-state reactions were carried out using a Retsch MM200 ball mill. A mixture of [MoO₂(HL)(MeOH)]Cl (0.0465 g, 0.10 mmol), *o*-vanillin azine (0.030 g, 0.15 mmol), and 30 μL of methanol were placed in a 10 mL Teflon milling jar with one 10 mm grinding ball. The reagents were milled for 60 min at a 25 Hz frequency. The obtained powder was rinsed with dry dichloromethane and dried. Yield: 46 mg, 76.7%.

Method B. [MoO₂Cl₂] (0.0597 g; 0.30 mmol) was added to the solution of H₂L (0.0814 g, 0.30 mmol) in 20 mL of dry methanol. Solution of *o*-vanillin azine (0.1352 g; 0.45 mmol) dissolved in dry CH₂Cl₂ (15 mL) was added to the resulting solution and it was then allowed to stand at room temperature for two days. The obtained red crystals of [1H]Cl·0.5VA were filtered, rinsed with dry dichloromethane, and dried in a desiccator up to a constant weight. Yield: 110 mg, 61.1%.

2.1.6. Synthesis of $[\text{MoO}_2(\text{HL})(\text{MeOH})]\text{Br}\cdot 0.5\text{VA}$ (**[1H]Br·0.5VA**)

Method A. The procedure was performed in the same manner as for **[1H]Cl·0.5VA** using **[1H]Br** (0.051 g, 0.10 mmol) and *o*-vanillin azine (0.030 g, 0.15 mmol). Yield: 59 mg, 91.6%.

Method B. The procedure was performed in the same manner as for **[1H]Cl·0.5VA** using $[\text{MoO}_2\text{Br}_2(\text{dmf})_2]$ (0.1302 g; 0.30 mmol), H_2L (0.0814 g, 0.30 mmol) and *o*-vanillin azine (0.1352 g; 0.45 mmol). Yield: 102 mg, 52.8%.

2.1.7. Synthesis of $[\text{MoO}_2(\text{HL})\text{Cl}]\cdot\text{MeOH}$ (**2Cl·MeOH**)

Method A. $[\text{MoO}_2\text{Cl}_2]$ (0.12 g, 0.60 mmol) was added to the solution of H_2L (0.16 g, 0.60 mmol) in 50 mL of dry methanol. The reaction mixture was left at room temperature. The corresponding product was filtered after one week and dried in a desiccator. Yield: 100 mg, 35.8%.

Method B. $[\text{MoO}_2(\text{acac})_2]$ (0.10 g, 0.31 mmol) was added to the solution of H_2L (0.090 g, 0.31 mmol) in 20 mL methanol. The temperature was lowered to 15 °C, and 150 μL of HCl ($w = 37\%$) was added to the resulting solution. The reaction mixture was stirred for half an hour and then left at room temperature. The obtained dark red crystals of **2Cl·MeOH** were filtered after five days, washed with ice-cold methanol and dried in a desiccator. Yield: 75 mg, 55.8%.

2.1.8. Synthesis of $[\text{MoO}_2(\text{HL})\text{Cl}]$ (**2Cl**)

$[\text{MoO}_2\text{Cl}_2]$ (0.12 g, 0.60 mmol) was added to a solution of H_2L (0.17 g, 0.60 mmol) in 50 mL of dry methanol in a quartz flask. The reaction mixture was irradiated with a UV light of 254 nm for two hours and then left at room temperature for five days. The supernatant solution was decanted in a dry box, and dry acetonitrile (25 mL) was added to crystals of **[1H]Cl·MeOH**. The suspension was allowed to stand at room temperature without stirring or shaking. Reaction and crystallization gradually proceeded, and finally, dark red crystals of **2Cl** were obtained. Yield: 82 mg, 31.5%

2.1.9. Synthesis of $[\text{MoO}_2(\text{HL})\text{Br}]\cdot 0.5\text{MeCN}$ (**2Br·0.5MeCN**)

$[\text{MoO}_2\text{Br}_2(\text{dmf})_2]$ (0.26 g, 0.60 mmol) was added to the solution of H_2L (0.17 g, 0.60 mmol) in 50 mL of dry methanol. The reaction mixture was left at room temperature overnight. The supernatant solution was decanted in a dry box, and dry acetonitrile (25 mL) was added to orange crystals of **[1H]Br**, and the suspension was allowed to stand at room temperature without stirring or shaking. Crystallization gradually proceeded, and finally, brown crystals of **2Br·0.5MeCN** were isolated. Yield: 75 mg, 25.1%

2.1.10. Synthesis of $[\text{MoO}_2(\text{L})(\text{MeOH})]$ (**1**)

The solution of Et_3N (35 μL) in dry methanol (50 mL) was cooled down to 0 °C, and $[\text{MoO}_2(\text{HL})\text{Cl}]\cdot\text{MeOH}$ (0.045 g, 0.10 mmol) was added. The suspension was left in a freezer at 5 °C. Reaction gradually proceeded, and finally after one week, crystals were filtered and dried in a desiccator. Yield: 31 mg, 72.2%.

2.1.11. Synthesis of $[\text{MoO}_2(\text{L})]_n$ (**2**)

A mixture of $[\text{MoO}_2(\text{acac})_2]$ (0.080 g, 0.25 mmol) and hydrazone H_2L (0.067 g, 0.25 mmol) in acetonitrile (10 mL) was placed in Teflon-lined autoclave and heated at 110 °C under autogenous pressure for 1.5 h. Crystals of $[\text{MoO}_2(\text{L})]_n$ (**2**) and $[\text{MoO}_2(\text{L})]_4$ were obtained concomitantly and manually separated for elemental analysis, ATR-IR, and SCXRD experiments.

2.2. Single Crystal and Powder X-ray Diffraction

The single-crystal X-ray diffraction (SCXRD) data of **[1H]Cl·MeOH**, **[1H]Br**, **[1H](ClA)_{0.5}·2MeOH**, **[1H]Cl·0.5VA**, **[1H]Br·0.5VA**, **2Cl·MeOH**, **2Cl**, **2Br·0.5MeCN**, **1** and **2** were collected by ω -scans on an Oxford Diffraction Xcalibur 3CCD diffractometer (Oxford Diffraction Ltd., Abingdon, UK) with graphite-monochromated MoK_α radiation or on an

XtaLAB Synergy-S diffractometer with CuK_α radiation (Rigaku Co., Tokyo, Japan). Data reduction was achieved using the CrysAlis software package [48]. Solution, refinement, and analysis of the structures were carried out using the programs integrated into the WinGX system [49]. The structures were solved by the direct methods using SHELXS and refined using the full-matrix least-squares method with the SHELXL program [50,51]. The non-hydrogen atoms were refined anisotropically. All hydrogen atoms were located unambiguously from difference Fourier maps. Because of poor geometry for some of them, they were placed in calculated positions and refined using the riding model. Exceptions were H atoms from the hydroxyl groups of the coordinated methanol molecules, which were restrained at $d(\text{O6}-\text{H61}) = 0.89(5)$ Å. Geometrical calculations were carried out using PLATON [52]. Drawings of the structures were prepared using the PLATON and MERCURY programs [53].

Crystals of all compounds harvested directly from the reaction mixture were suitable for the SCXRD experiments. The asymmetric units and crystal structures of **[1H]Cl**·MeOH, **[1H]Br**, **[1H](ClA)_{0.5}**·2MeOH, **[1H]Cl**·0.5VA, **[1H]Br**·0.5VA, **2Cl**·MeOH, **2Cl**, **2Br**·0.5MeCN, **1** and **2** are shown in Figure S1 and Figure S2, respectively, Supplementary Materials. Details for the structure solution and refinement for all compounds are tabulated in Tables S1 and S2, Supplementary Materials. Selected bond lengths and angles are summarized in Tables S3–S7, Supplementary Materials.

The powder X-ray diffraction (PXRD) data were collected using a Malvern Panalytical Aeris powder diffractometer (Malvern Panalytical B.V., Almelo, The Netherlands) in the Bragg-Brentano geometry with a PIXcel^{1D} detector, using CuK_α radiation ($\lambda = 1.5406$ Å). Samples were contained on a Si sample holder. Powder patterns were collected at room temperature in the range of 5–40° (2θ). The data were collected and visualized utilizing the Malvern Panalytical HighScore Software Suite [54].

2.3. Thermal and Spectroscopic Measurements

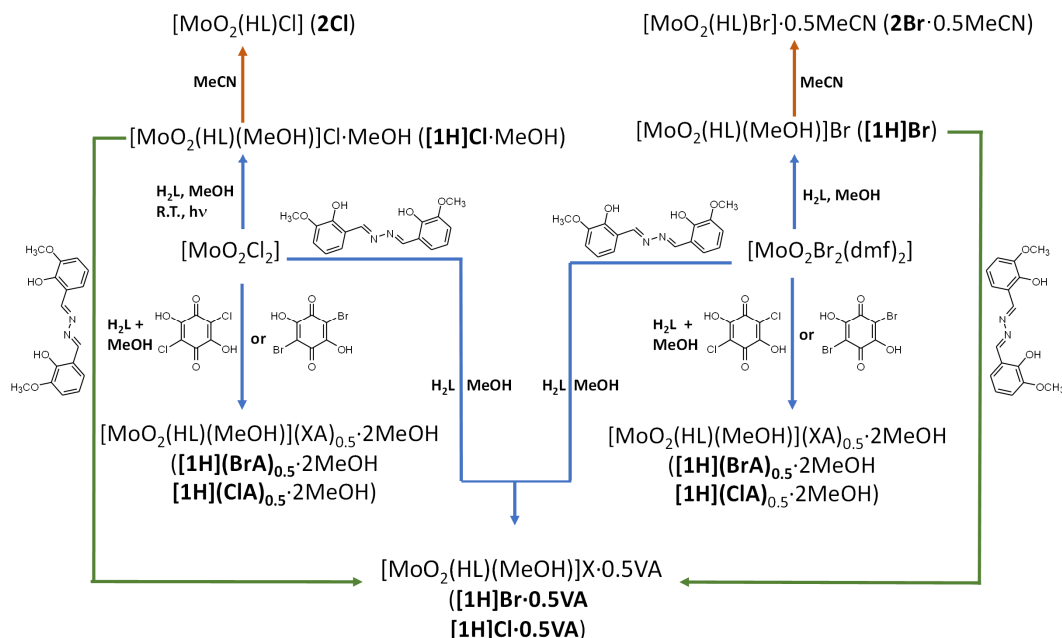
Thermogravimetric (TG) analyses were carried out using a Mettler TG 50 thermobalance (Mettler Toledo, Columbus, OH, USA) using Al_2O_3 crucibles under an oxygen stream in a temperature range between 25 °C and 600 °C. The heating rate was adjusted to 5 °C min^{-1} . The results of TG experiments were evaluated using the Mettler Toledo STARe evaluation software (version 16.10). Attenuated Total Reflectance Infrared (ATR-IR) spectra were acquired on a Perkin Elmer Spectrum One spectrometer (Waltham, MA, USA). The solid-state nuclear magnetic resonance (NMR) spectra were recorded on Bruker Avance Neo 300 spectrometer (Bruker Biospin GmbH; Rheinstetten, Germany) equipped with a 4 mm broad band magic angle spinning (MAS) probe. The samples for ^{13}C CP-MAS spectra were spun at the magic angle of 10 kHz. The spectra were acquired with 1024 scans, contact time of 2 ms, and repetition delay of 7 s. The ^1H NMR spectra were recorded in $\text{dms-}d_6$ on a Bruker Avance NEO 300 NMR spectrometer operating at 300 MHz for ^1H and 75 MHz for ^{13}C using a C/H dual 5 mm probe. The spectra were recorded with a sample concentration of 20 mg mL^{-1} . TMS was used as the internal standard. ^1H NMR spectra with spectral width of 6200 Hz and a digital resolution of 0.09 Hz per point were measured with 32 scans. APT spectra with spectral widths of 18,030 Hz were collected with 10,240 scans. Digital resolution was 0.55 Hz per point.

2.4. In Vitro Cytotoxic Activity

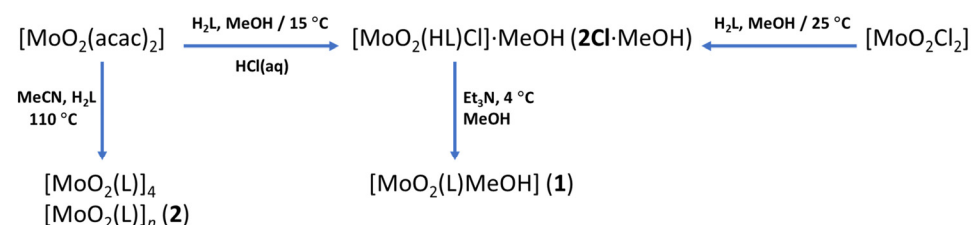
The cytotoxicity of selected compounds, namely **[1H]Cl**, **[1H](ClA)_{0.5}**, **[1H]Cl**·0.5VA, **2Cl** and **1**, was assessed on human acute monocytic leukemia (THP-1, ATCC TIB-202) and hepatocellular carcinoma (HepG2, ATCC HB-8065) cells. The cell growth and cytotoxicity assay were performed according to the previously reported protocols [46]. Briefly, each cell line was exposed to various concentrations of the tested compounds and the cell viability after exposure was determined using the MTS assay [55]. The half maximal inhibitory concentration (IC_{50}) values were calculated from dose-response curves. All experiments were performed in duplicate.

3. Results and Discussion

The overview of all product types, complex salts, solvates, and co-crystals, as well as deprotonated coordination compounds, is given in Schemes 2 and 3.



Scheme 2. The reaction scheme for the synthesis of complex salts, solvates, and co-crystals (H_2L = hydrazone ligand, $X^- = Cl^-$ or Br^- , XA^{2-} = chloranilate or bromanilate, VA = *o*-vanillin azine). The reactions depicted by blue arrows were performed in dry solvents, while those depicted by green arrows were carried out mechanochemically. Structural transformations are shown by orange arrows.



Scheme 3. The reaction scheme for the synthesis of neutral mononuclear, tetranuclear, and polynuclear complexes.

3.1. Complex Salts, Solvates and Co-Crystals—Synthesis of $[1H]X$, $[1H](XA)_{0.5} \cdot 2MeOH$, and $[1H]X \cdot 0.5VA$ ($X = Cl$ or Br , $XA = ClA$ or BrA)

Compound $[MoO_2(HL)(MeOH)]Cl \cdot MeOH$ (**[1H]Cl·MeOH**) was successfully obtained when the reaction mixture of hydrazone and $[MoO_2Cl_2]$ in dry methanol was exposed to UV light at ambient temperature. Without UV irradiation the reaction afforded complex $[MoO_2(HL)Cl] \cdot MeOH$ (**2Cl·MeOH**). Solvate **2Cl·MeOH** was also obtained utilizing $[MoO_2(acac)_2]$ as a precursor in reaction with H_2L in the presence of a small amount of hydrochloric acid (Scheme 2). However, $[MoO_2Br_2(dmf)_2]$ reacting with H_2L in methanol yielded $[MoO_2(HL)(MeOH)]Br$ (**[1H]Br**), and bromide coordination was not observed, which was ascribed to different donor strength of the bromide.

The reaction of $[MoO_2Cl_2]$ or $[MoO_2Br_2(dmf)_2]$ and H_2L in a 1:1 molar ratio in the presence of chloranilic or bromanilic acid afforded $[MoO_2(HL)(MeOH)](XA)_{0.5} \cdot 2MeOH$ (**[1H](ClA)_{0.5}·2MeOH** or **[1H](BrA)_{0.5}·2MeOH**) assemblies. Comparison of their ATR-IR spectra with those of H_2XA and $[MoO_2(HL)(MeOH)]^+$ components (Figure S3, Supplementary Materials) revealed that they couldn't be considered as neutral co-crystals but as complex salts. The spectra of **[1H](XA)_{0.5}·2MeOH** displayed strong bands around 1495 cm^{-1} , at-

tributable to the $C^{\cdots}O_{XA}$ stretching vibrations, indicating the delocalization of π -electrons in anions (Scheme S1) [34], and the structure of anion with four short C–O bond distances (Table S3), which was confirmed by SCXRD. $[1H](CIA)_{0.5} \cdot 2MeOH$ and $[1H](BrA)_{0.5} \cdot 2MeOH$ exhibited similar PXRD patterns and ATR-IR spectra clearly due to similarity in their solid-state structures (Figure S4, Supplementary Materials). They represent the first examples of Mo(VI) complex salts with such anions.

Reactions with chloranilic and bromanilic acids were also performed with different molar ratios (from 1:1.5 to 1:5). Nevertheless, the obtained products were always $[1H](XA)_{0.5} \cdot 2MeOH$. Also, reactions utilizing the mechanochemical synthesis with a small amount of methanol failed to produce extended supramolecular structures $\{[MoO_2(HL)(MeOH)](XA)_{0.5} \dots H_2XA \dots\}_n$ or $\{[MoO_2(HL)(MeOH)](HXA) \dots H_2XA \dots\}_n$.

In order to further examine the formation of multi-component materials, we selected *o*-vanillin azine. The reaction of $[1H]Cl \cdot MeOH$ or $[1H]Br$ with VA, applying the mechanochemical procedure, afforded the 1:0.5 assemblies $[MoO_2(HL)(MeOH)]X \cdot 0.5VA$ ($[1H]Cl \cdot 0.5VA$ or $[1H]Br \cdot 0.5VA$, respectively). The crystals suitable for the SCXRD experiment were obtained by the reaction of $[MoO_2Cl_2]$ or $[MoO_2Br_2(dmf)_2]$ with H_2L and VA utilizing the solution-based method. Their bulk samples were compared using the PXRD method, Figure 1. Also, the stretching vibrations belonging to *o*-vanillin azine in the ATR-IR spectra of $[1H]Cl \cdot 0.5VA$ and $[1H]Br \cdot 0.5VA$ (assigned to $-CH=N_{VA}$ and $C-O_{VA}$ at 1623 cm^{-1} and 1243 cm^{-1} , respectively), varied in intensity when compared to the spectrum of free azine. These findings were consistent with the formation of co-crystals (Figure S5, Supplementary Materials).

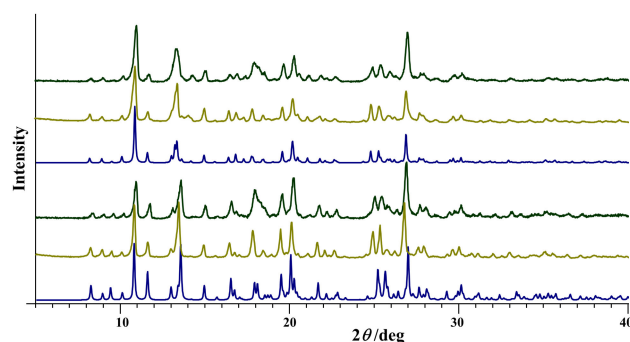


Figure 1. PXRD patterns of $[1H]Cl \cdot 0.5VA$ (the three powder patterns on the top) and $[1H]Br \cdot 0.5VA$ (the three powder patterns on the bottom) obtained by the mechanochemical method (the dark green lines) and solution-based method (the olive lines). The blue lines indicate patterns calculated from the X-ray single-crystal structures of the corresponding co-crystals.

3.2. Counter Anion Effects and Transformation of Complex Assemblies—Synthesis of **2Cl** and **2Br·0.5MeCN**

Although salts $[1H]Cl \cdot MeOH$ and $[1H]Br$ are thermally very stable (see Section 3.6), they are extremely unstable in the air. Once exposed to humidity, the orange crystals became brittle and finally developed a dark red color. Compared to halide salts, co-crystals with *o*-vanillin azine $[1H]Cl \cdot 0.5VA$ and $[1H]Br \cdot 0.5VA$ were stable at ambient conditions indefinitely. Their different behaviour could be ascribed to differences in crystal packing (see Section 3.4.1).

When crystals of $[1H]Cl \cdot MeOH$ or $[1H]Br$ were immersed in dry acetonitrile and the suspension left at room temperature, a structural transformation occurred and resulted in the formation of $[MoO_2(HL)Cl]$ (**2Cl**) and $[MoO_2(HL)Br] \cdot 0.5MeCN$ (**2Br·0.5MeCN**), respectively (Scheme 2). The coordination of halide to *cis*- $[MoO_2]^{2+}$ unit resulted in a colour change from orange to dark red in the case of chloride and from deep orange to reddish-brown in the case of bromide (Figure 2a). The complete crystallization process was confirmed by PXRD analysis after two weeks (Figure 2b).

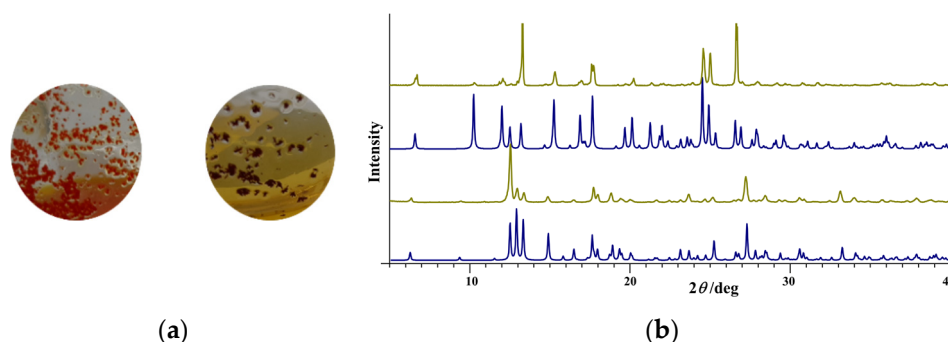


Figure 2. (a) Photographs of $[1H]Br$ in MeOH (left) and $2Br \cdot 0.5MeCN$ in acetonitrile (right). (b) PXRD patterns of $[1H]Br$ (top) and $2Br \cdot 0.5MeCN$ (bottom). The olive lines indicate patterns obtained by powder diffraction, while the blue lines indicate patterns calculated from the X-ray single-crystal structures of the corresponding compounds.

On the other hand, crystals of $[1H](ClA)_{0.5} \cdot 2MeOH$ or $[1H](BrA)_{0.5} \cdot 2MeOH$ in acetonitrile transformed into the $[1H](ClA)_{0.5}$ and $[1H](BrA)_{0.5}$, respectively, and no further loss or replacement of the coordinated methanol molecules was observed. PXRD patterns of the lattice solvent-free residuals revealed their lower crystallinity.

3.3. Deprotonated Mo-Hydrazone Assemblies—Synthesis of **1** and **2**

In order to further explore these complexes, triethylamine was added to the methanolic solution of $[MoO_2(HL)Cl] \cdot MeOH$ (**2Cl**·MeOH) while maintaining a temperature around 0 °C. Ligand deprotonation was accompanied by chloride substitution resulting in the new polymorphic form of $[MoO_2(L)(MeOH)]$ (**1**), Figure 3. The same product was obtained from $[MoO_2(HL)Br] \cdot 0.5MeCN$ (**2Br**·0.5MeCN). These transformations were clearly seen in the ATR-IR spectra. A broad band in the range 2400–2700 cm^{-1} , assigned to the $N_{py}-H$ stretching vibrations, present in the spectra of compounds comprising singly-deprotonated hydrazone ligand was missing in the spectrum of **1**.

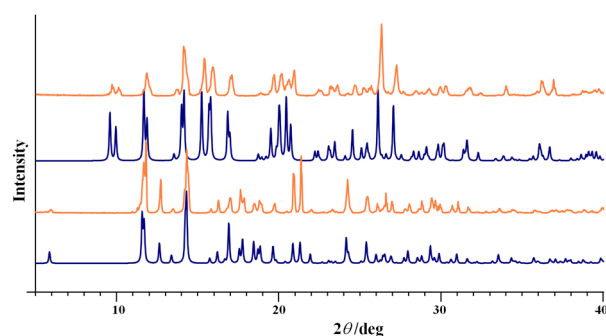


Figure 3. PXRD patterns of $[MoO_2(L)(MeOH)]$ polymorphs: (top) obtained by reaction of H_2L with $[MoO_2(acac)_2]$, (bottom) obtained by sample obtained upon deprotonation of $[1H]Cl \cdot MeOH$. The orange lines indicate patterns obtained by powder diffraction, while the blue lines indicate patterns calculated from the X-ray single-crystal structures of the corresponding polymorphs.

On the other hand, the reaction of H_2L with $[MoO_2(acac)_2]$ as a precursor in methanol yielded previously published polymorph of $[MoO_2(L)(MeOH)]$ [56–58]. Moreover, the reaction of H_2L with $[MoO_2(acac)_2]$ conducted under solvothermal conditions in acetonitrile at a temperature of 110 °C afforded a mixture of the tetrameric $[MoO_2(L)]_4$ [9] and polymeric $[MoO_2(L)]_n$ (**2**) supramolecular isomers. The products deposited concomitantly from the heated reaction mixture and not upon subsequent cooling. All attempts to obtain pure coordination polymer failed.

3.4. Crystallographic Studies

3.4.1. Structures of the Complex Salts, Solvates and Co-Crystals [1H]X, [1H](XA)_{0.5}·2MeOH, and [1H]X·0.5VA (X = Cl or Br, XA = CIA or BrA)

Complex cation [MoO₂(HL)(MeOH)]⁺ ([1H]⁺) is present in all salts ([1H]Cl·MeOH, [1H]Br, [1H](CIA)_{0.5}·2MeOH) and also in isostructural multicomponent assemblies ([1H]Cl·0.5VA and [1H]Br·0.5VA). The ligand is in the HL[−] form and is coordinated to the *cis*-[MoO₂]²⁺ core in the tridentate mode via the *ONO* donor atoms. The sixth coordination site is occupied by the O atom from the coordinated methanol molecule. The distance Mo–O_{MeOH} represents the largest bond length within the distorted octahedron (Tables S3 and S4).

In the crystal structures of [1H]Cl·MeOH and [1H]Br salts, the halide anions and the complex cations [1H]⁺ are connected through a bifurcated hydrogen bonds involving the pyridine nitrogen atom (N3–H3···Cl1[−1/2+x,1/2+y,z] = 3.071(2) Å in [1H]Cl·MeOH, N3–H3···Br1[x,−1+y,z] = 3.1604(18) Å in [1H]Br) and the oxygen atom from the coordinated methanol molecule (O6–H61···Cl1[1/2−x,1/2+y,1/2−z] = 3.0034(19) Å in [1H]Cl·MeOH, and O6–H61···Br1[x,−1+y,z] = 3.2040(14) Å in [1H]Br) forming dimers related via 2-fold axis in [1H]Cl·MeOH (Figure 4a) and infinite 1D chains in [1H]Br (Figure 4b). In [1H]Cl·MeOH the dimers are further connected through the N3–H3···O1[−1/2+x,−1/2+y,z] = 3.037(3) Å hydrogen bond thus forming an infinite 2D network (Figure 4a, Table S7). Within each chain in [1H]Br there are π -stacking interactions, whereas neighbouring chains are connected by C–H···Br, C–H···O hydrogen bonds and π -stacking interactions between the pyridyl and the phenyl ring (Table S7). Solvate methanol molecule in [1H]Cl·MeOH is equally disordered over two positions and the oxygen atom O7 of the disordered methanol molecule forms a weak hydrogen bond with O4 of the five membered chelate ring (O7···O4) and with the chloride anion (O7···Cl1[1/2−x,1/2+y,1/2−z]) from the dimer of the surrounding layer with the length of 3.213(5) Å and 3.365(4) Å, respectively.

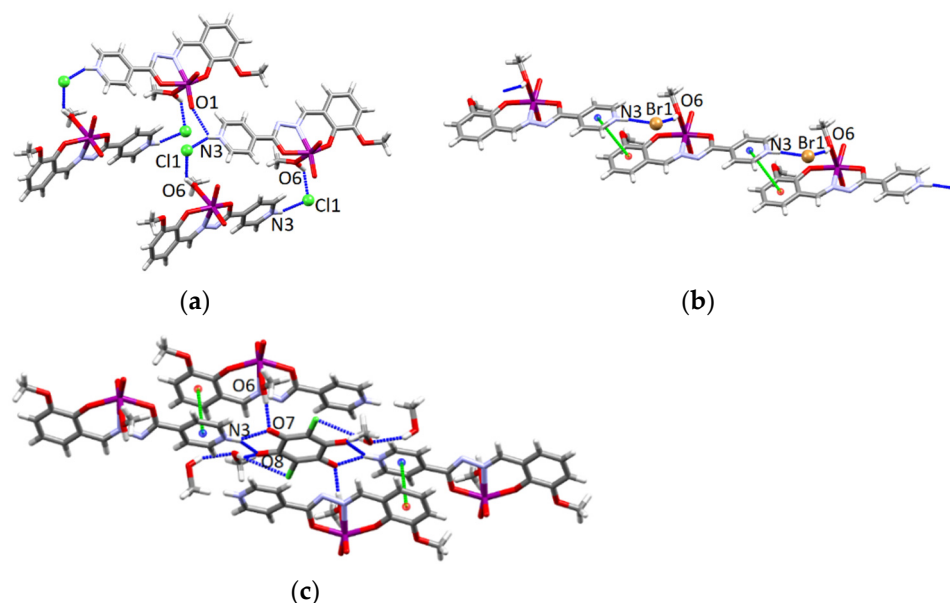


Figure 4. (a) Two dimers in [1H]Cl·MeOH formed through N3–H3···Cl1 and O6–H61···Cl1 hydrogen bonds and connected by N3–H3···O1 hydrogen bond, (b) Infinite 1D chain in [1H]Br formed through O6–H61···Br1 and N3–H3···Br1 hydrogen bonds, (c) 2D network in [1H](CIA)_{0.5}·2MeOH formed by N3–H3···O7, N3–H3···O8, O6–H6···O7 hydrogen bonds. Hydrogen bonds are shown by blue dotted lines. Green dashed lines indicate π -stacking interactions (Cg3 is centre of gravity of the pyridyl ring, blue spheres and Cg4 is centre of gravity of the phenyl ring, red spheres).

In [1H](CIA)_{0.5}·2MeOH salt, the anion is located on an inversion centre, so that the asymmetric unit contains one complex cation, one half of the chloranilate anion and two methanol

molecules of crystallization (Figure S1). Each ClA^{2-} anion is hydrogen bonded to four $[\mathbf{1H}]^+$ cations involving the pyridine nitrogen atom ($\text{N3-H3} \cdots \text{O7}[-1+x,y,z] = 2.730(3) \text{ \AA}$ and $\text{N3-H3} \cdots \text{O8}[-x,2-y,1-z] = 2.893(3) \text{ \AA}$) and the oxygen atom from the coordinated methanol molecule ($\text{O6-H6} \cdots \text{O7} = 2.640(3) \text{ \AA}$) thus forming a 2D layers (Figure 4c). One methanol molecule of crystallization is linked to the chloranilate anion by two hydrogen bonds ($\text{O9-H9A} \cdots \text{O8} = 2.834(3) \text{ \AA}$ and $\text{O9-H9A} \cdots \text{Cl1} = 3.559(4) \text{ \AA}$) and with the second methanol molecule of crystallization by the hydrogen bond $\text{O10-H1A} \cdots \text{O9} = 2.893(4) \text{ \AA}$. The layers are further connected through $\text{C-H} \cdots \text{Cl}$, $\text{C-H} \cdots \text{O}$ hydrogen bonds and π -stacking interactions between the pyridyl and the phenyl ring (Table S7).

The asymmetric unit of both isostructural compounds $[\mathbf{1H}]\text{Cl}\cdot\mathbf{0.5VA}$ and $[\mathbf{1H}]\text{Br}\cdot\mathbf{0.5VA}$ contains the complex cation, halide anion, and one half of the *o*-vanillin azine molecule (Figure S1). The VA molecule possesses an inversion centre, and it is almost planar with the central C=N-N=C unit in the (*E,E*) conformation, which is in accordance with the previously reported VA crystal structures [38,59]. A pair of six-membered rings formed through intramolecular $\text{O7-H71} \cdots \text{N4}$ hydrogen bonds are present in the terminal vanillin-imine moieties (Figure 5).

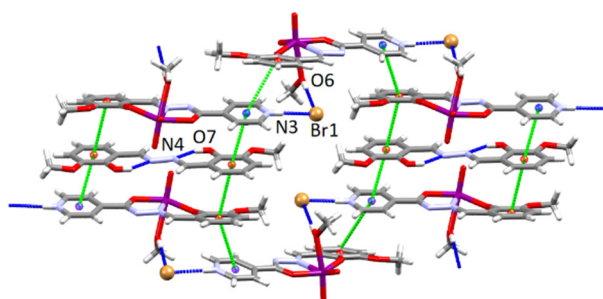


Figure 5. The crystal packing of the $[\mathbf{1H}]\text{Br}\cdot\mathbf{0.5VA}$. Intramolecular $\text{O7-H71} \cdots \text{N4}$ and intermolecular hydrogen bonds $\text{O6-H61} \cdots \text{Br1}$ and $\text{N3-H3} \cdots \text{Br1}$ are shown by blue dotted lines. Green dashed lines indicate π -stacking interactions (Cg3 is centre of gravity of the pyridyl ring, blue spheres and Cg4 and Cg5 are centres of gravity of the phenyl ring, red spheres).

In $[\mathbf{1H}]\text{X}\cdot\mathbf{0.5VA}$ the halide anion links two complex cations through a bifurcated hydrogen bond involving the pyridine nitrogen atom ($\text{N3-H3} \cdots \text{Cl1}[1-x,1/2+y,1/2-z] = 2.995(2) \text{ \AA}$ in $[\mathbf{1H}]\text{Cl}\cdot\mathbf{0.5VA}$, $\text{N3-H3} \cdots \text{Br1} = 3.1496(17) \text{ \AA}$ in $[\mathbf{1H}]\text{Br}\cdot\mathbf{0.5VA}$) and the oxygen atom from the coordinated methanol molecule ($\text{O6-H61} \cdots \text{Cl1} = 3.013(2) \text{ \AA}$ in $[\mathbf{1H}]\text{Cl}\cdot\mathbf{0.5VA}$, and $\text{O6-H61} \cdots \text{Br1}[1-x,1/2+y,1/2-z] = 3.1805(14) \text{ \AA}$ in $[\mathbf{1H}]\text{Br}\cdot\mathbf{0.5VA}$) forming an infinite 1D chain. In both crystal structures the *o*-vanillin azine molecules are positioned between the chains of complex cations and halide anions and stabilized by π -stacking interactions with very short centroid-centroid distances between pyridyl and phenyl rings (Figure 5, Table S8). $\text{C-H} \cdots \text{O}$ interactions between the vanillin azine molecules and complex cations are also observed (Table S8).

3.4.2. Structures of the Neutral Complexes $\mathbf{2Cl}$, $\mathbf{2Cl}\cdot\text{MeOH}$ and $\mathbf{2Br}\cdot\mathbf{0.5MeCN}$

In all three complexes $\mathbf{2Cl}$, $\mathbf{2Cl}\cdot\text{MeOH}$ and $\mathbf{2Br}\cdot\mathbf{0.5MeCN}$, 2D network is formed through the different pattern of hydrogen bonds. In $\mathbf{2Cl}$, complex molecules are hydrogen bonded through the $\text{N3-H3} \cdots \text{Cl1} [1/2+x,1/2-y,-1/2+z] = 3.062(3)$ and $\text{N3-H3} \cdots \text{O2}[1+x,y,z] = 2.955(4) \text{ \AA}$ bonds in which the protonated nitrogen atom of the isonicotinyl moiety acts as a hydrogen bond donor while the coordinated chloride anion and the terminal oxygen atom act as acceptors (Figure 6a) and form an infinite 2D network.

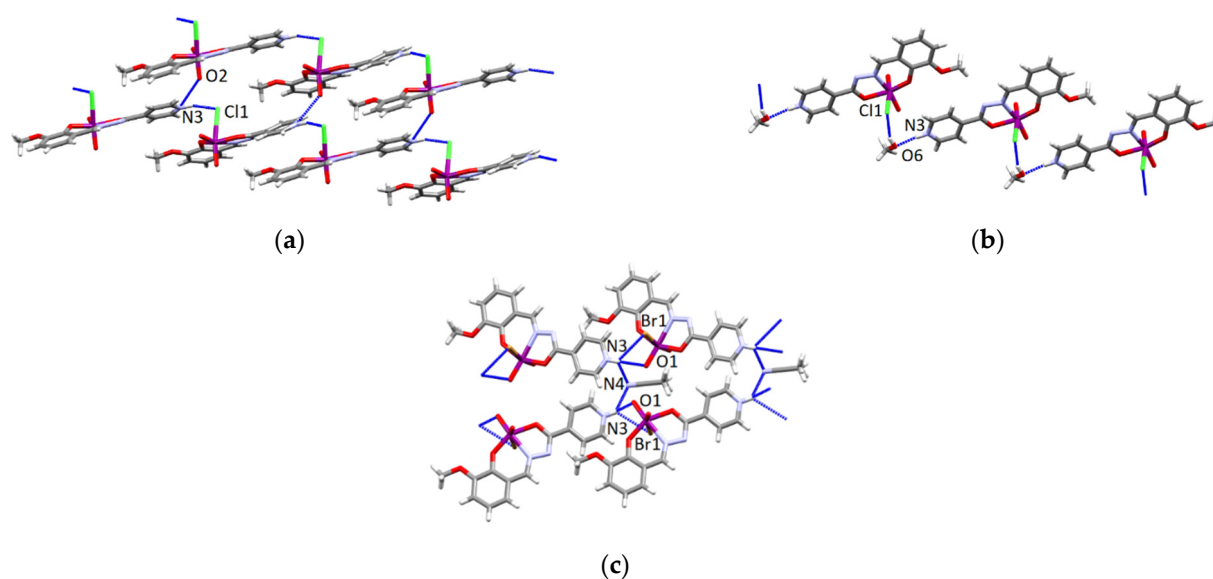


Figure 6. (a) 2D network in **2Cl** formed by $N3-H3 \cdots Cl1$ and $N3-H3 \cdots O2$ hydrogen bonds. (b) Infinite 1D chain formed by $N3-H3 \cdots O6$ and $O6-H6A \cdots Cl1$ hydrogen bonds in **2Cl**·MeOH. (c) 2D network in **2Br**·0.5MeCN formed by $N3-H3 \cdots O1$, $N3-H3 \cdots Br1$ and $N3-H3 \cdots N4$ hydrogen bonds. Hydrogen bonds are shown by blue dotted lines.

In **2Cl**·MeOH, the methanol molecule of crystallization connects two complex molecules through the hydrogen bonds involving the nitrogen atom of the pyridyl ring and the coordinated chloride anion ($N3-H3 \cdots O6[x, -1+y, z] = 2.730(3)$, $O6-H6A \cdots Cl1[1+x, y, z] = 3.227(2)$ Å) forming an infinite 1D chains (Figure 6b). Neighbouring chains are connected by $C-H \cdots Cl$, $C-H \cdots O$ interactions and π -stacking interactions between the pyridyl and the phenyl ring (Table S9 and Figure S2) forming the 2D network. In **2Br**·0.5MeCN, complex molecules are connected through the protonated nitrogen atom of the isonicotinyl moiety as a hydrogen bond donor and terminal oxygen and coordinated bromide ion as acceptors ($N3-H3 \cdots O1[x, 1+y, z] = 3.038(4)$ Å, $N3-H3 \cdots Br1[x, 1+y, z] = 3.574(3)$ Å) forming 1D chains (Figure 6c). Furthermore, neighbouring 1D chains are connected by the bifurcated hydrogen bond involving the nitrogen atom from the acetonitrile solvent molecule and the protonated pyridine nitrogen atom ($N3-H3 \cdots N4[x, 1+y, z] = 3.057(3)$ Å) making an infinite 2D network (Figure 6c). Additionally, in **2Cl** and **2Br**·0.5MeCN, 2D networks are stabilized by π -stacking interactions between the phenyl and pyridyl ring or between the two phenyl rings, respectively (Table S9), and by $C-H \cdots O$ and $C-H \cdots X$ ($X = Cl, Br$) interactions (Table S9).

3.4.3. Structures of the Deprotonated Mo-Hydrazone Assemblies **1** and **2**

The distorted octahedral coordination of each molybdenum in **1** and **2** is completed by the solvent oxygen atom or isonicotinoyl nitrogen, respectively. These bonds are weaker which is reflected in the lengthening of the $Mo-O6$ and $Mo-N3'$ distances (Table S6). In complex **1**, the characteristic feature is formation of the hydrogen bonded 1D chains in which molecules are connected via $O6-H61 \cdots N3[x, -1+y, z] = 2.702(4)$ Å hydrogen bond (between the hydroxyl group of the coordinated methanol molecule and the nitrogen atom of a pyridine ring), Figure 7a. For comparison, in the crystal structure of the previously reported polymorph the molecules form discrete centrosymmetric dimers (CSD refcode KANYIJ, KANYIJ01, KANYIJ02) [56–58]. The coordination polymer **2** consists of infinite 1D zig-zag chains (Figure 7b). This architecture is tightly enough packed to exclude solvent molecules. There are no classical hydrogen bonds in the polymer crystal structure, however, the polymeric chains are stabilized by weak intermolecular $C-H \cdots O$ hydrogen bonds (Table S10). In **1** and **2**, there are also π -stacking interactions between the pyridyl and the phenyl ring (Figure 7 and Table S6).

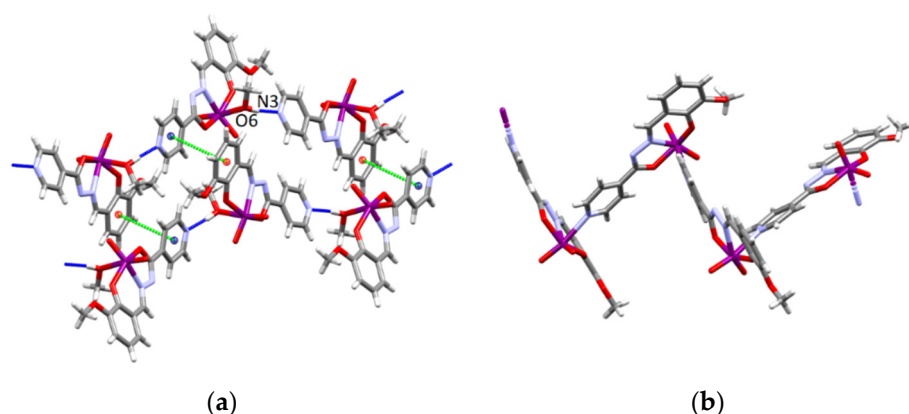


Figure 7. (a) Infinite 1D chains in **1** formed through O6–H61···N3 hydrogen bonds. (b) Infinite zig-zag chain in the crystal structure of **2**. Hydrogen bonds are shown by blue dotted lines. Green dashed lines indicate π -stacking interactions (Cg3 is centre of gravity of the pyridyl ring, blue spheres and Cg4 is centre of gravity of the phenyl ring, red spheres).

3.5. Spectroscopic Studies

All complexes were characterized by NMR spectral data (Scheme S1, Tables S8–S13, Supplementary Materials). The proton and carbon chemical shifts were assigned utilizing one- and two-dimensional NMR techniques. Results are in accordance with previous findings for the similar Mo-hydrazone compounds derived from 3-methoxy salicylaldehyde [18–20]. The solution and solid-state NMR spectra are shown in Figures S6–S12, Supplementary Materials.

The most deshielded peaks, detected between 165.71 ppm and 168.05 ppm, were attributed to the carbon atoms at position 6 (belonging to the hydrazone C–O group). The methyl protons and carbons were found at around ~3.8 ppm and ~56 ppm. Observed differences in NMR chemical shifts pointed towards isonicotinoyl nitrogen atom protonation. NH protons experienced different chemical shift values, indicating their involvement in hydrogen bonding interactions. In solution, aromatic carbons were found to resonate in the range 117–151 ppm (Tables S8–S10), while in the solid state were observed in the range 117–175 ppm (Tables S11–S13), as a consequence of different properties of samples in different environments. In **1**, the broad signal belonging to the protonated isonicotinoyl NH was missing indicating formation of the deprotonated complex (Table S10). The comparison of NMR spectrum of **1** and spectra of metallosupramolecular assemblies suggested that they were all mononuclear complexes with dms- d_6 coordinated to MoO₂²⁺ core. Their spectra did not change with time. On the contrary, the additional peaks in the spectra of the complex salts were noticed (Figure S12). These results indicate a different stability of the complexes due to complex salts interaction with moisture during sample preparation for the NMR experiment.

Changes in the chemical shifts in the solution and solid-state spectra were detected for carbons at positions 2–5 in the pyridine ring. Detected differences were influenced by the crystal packing. Tentative assignments were carried out based on the NMR data obtained in the solution (Tables S11–S13, Supplementary Materials). In the solid state, the main differences between [1H]Cl and [1H]Br complexes and co-crystals with *o*-vanillin azine, [1H]Cl·0.5VA and [1H]Br·0.5VA, respectively, were observed for methyl carbons and carbon atoms at positions 3, 4, and 9 as a consequence of electron redistribution upon the interaction of complex salts with *o*-vanillin azine and influence of halide anions (Figure S10). The solid state ¹³C CP-MAS spectra of [1H]Cl·0.5VA and [1H]Br·0.5VA were also compared. The chemical shift values showed similarities between them thus corroborating their isostructural nature.

The isonicotinoyl nitrogen protonation in the complex salts displayed a correspondingly small effect on the hydrazone C–O and imine C=N carbon atoms shifts (at positions 6 and 7, respectively). Additionally, coordination of halide in 2Cl·MeOH and

2Br·0.5MeCN also affected the chemical shifts upfield and downfield relative to neutral complex **1** (Figure S11). These differences in chemical shift values were ascribed to different donor strengths of the halide and methanol co-ligands, and consequently, different electron redistribution within the complex. Therefore, the ^{13}C CP-MAS NMR data could be useful to verify the co-ligand in the coordination sphere of the metal centre.

3.6. Thermogravimetric Studies

TG curves are given in Figures S13–S15, Supplementary Materials. TG study of **[1H]Cl**·MeOH and **[1H]Br** revealed that the loss of the lattice and coordinated methanol molecules was accompanied by the release of HCl and HBr in the range 109–144 °C and 170–190 °C, respectively. However, in the case of **[1H]Cl**·0.5VA and **[1H]Br**·0.5VA, the first change in the sample mass was attributed to the coordinated MeOH molecule release (in the range 78–118 °C, and 100–138 °C, respectively). The loss of HCl/HBr, and decomposition of VA, were accompanied by the thermal decomposition of the hydrazone ligand.

On the other hand, crystals of **[1H](XA)**_{0.5}·2MeOH were transformed into the salts **[1H](XA)**_{0.5} already at room temperature, through the loss of the lattice solvent molecules. When **[1H](ClA)**_{0.5}·2MeOH and **[1H](BrA)**_{0.5}·2MeOH were heated in the oxygen atmosphere, the mass loss due to the release of the lattice and coordinated methanol molecules occurred in the range 25–207 °C and 25–171 °C, respectively.

Complexes **2Cl**·MeOH, **2Br**·0.5MeCN, and **1** exhibited a first weight loss (in the range 117–142 °C, 172–195 °C, and 139–160 °C, respectively) corresponding to the release of the lattice and coordinated solvent molecule, respectively. The decomposition of the residual occurred in the range 206–503 °C for **2Cl**, and 267–531 °C for **1**.

3.7. Cytotoxicity

The results of the cell viability assay are presented in Table 1. Based on the high IC₅₀ values, all tested compounds can be considered noncytotoxic against HepG2 cell line. Substantial cytotoxic activity of the compounds was established on THP-1 cells. Moreover, compounds **[1H]Cl**, **2Cl** and **1** exhibited similar activity against both HepG2 and THP-1 cells as the related dioxomolybdenum(VI) compounds with 4-methoxysalicylaldehyde isonicotinoyl hydrazone [27]. The substitution of chloride by chloranilate as well as the introduction of *o*-vanillin azine in **[1H]Cl** resulted in somewhat lowered cytotoxicity.

Table 1. Cytotoxicity of the tested compounds.

Compound	IC ₅₀ /μmol L ⁻¹	
	HepG2	THP-1
[1H]Cl	98.33	2.77
[1H](ClA) _{0.5}	>100	26.7
[1H]Cl ·0.5VA	>100	29.2
2Cl	>100	3.21
1	>100	4.54
staurosporine	14.31	0.18

4. Conclusions

We have synthesized and characterized a series of Mo(VI) hydrazone complex salts, solvates, co-crystals, and neutral complexes. Different supramolecular architectures are produced depending on the nature of the counter anions and solvent molecules. Anions (chloride/bromide) in the complex salts **[1H]Cl**·MeOH and **[1H]Br** connects complex cations [MoO₂(HL)(MeOH)]⁺ (**[1H]**⁺) through the pyridine nitrogen atom and oxygen atom from the coordinated methanol molecule by using different patterns of H-bond motifs. They both participate in the formation of isostructural co-crystals **[1H]Cl**·0.5VA and **[1H]Br**·0.5VA, in which non-bonding interactions facilitate the incorporation of the *o*-vanillin azine into the complex salt network.

When the chloranilic or bromanilic acid is used, halide substitution occurs, resulting in the formation of the Mo-complex salts of the general formula $[1H](XA)_{0.5} \cdot 2MeOH$. The addition of the acid in excess failed to produce a multicomponent network of general composition $\{[MoO_2(HL)(MeOH)](XA)_{0.5} \dots H_2XA \dots\}_n$ that can compete with the stability of the complex salts $[1H](XA)_{0.5} \cdot 2MeOH$. It seems that the packing arrangements within the crystal structures, the relative orientation of cations $[1H]^+$ and XA^{2-} anions and interactions between them contribute to their stability.

Despite high thermal stability, the compounds $[1H]Cl \cdot MeOH$ and $[1H]Br$ are very sensitive to moisture upon standing in the air. Furthermore, when $[1H]Cl \cdot MeOH$ and $[1H]Br$ are immersed in a weak donor solvent, such as dry acetonitrile, the methanol is replaced with halide and complexes $[MoO_2(HL)X]$ (**2Cl** and **2Br**·0.5MeCN) are formed. Solvate **2Cl**·MeOH is also obtained from methanol depending on the reaction conditions. These changes in the coordination sphere of Mo results in a significant colour change. Similar behaviour with $[1H](XA)_{0.5}$ is not observed. That can be rationalised by understanding the differences between the anions' coordinating characteristics.

According to the results the coordinating ability of the anions toward Mo(VI) varies in the order $Cl > Br > XA$. In the presence of a weak base, the anions are not included in the structure. The neutral networks of $[MoO_2(L)(MeOH)]$ (**1**), and metallosupramolecular tetrameric $[MoO_2(L)]_4$ and polymeric $[MoO_2(L)]_n$ (**2**) isomers are formed depending on the reaction conditions. Solvent choice and reaction temperature play an important structure-directing role.

Supplementary Materials: The following supporting information can be downloaded at: <https://www.mdpi.com/article/10.3390/cryst12040443/s1>. Figure S1: The asymmetric units of compounds; Tables S1 and S2: Crystallographic data and structure refinement data; Tables S3–S6: Selected bond lengths and angles; Tables S7–S10: Geometry of hydrogen bonds and π -interactions; Figure S2: Crystal structures; Analytical data for compounds; Figures S3–S5: IR-ATR spectra; Scheme S1: Structure and the NMR numbering scheme; Tables S8–S10: 1H and ^{13}C chemical shifts of compounds in $dmsO-d_6$; Tables S11–S13: Tentative assignment of ^{13}C CP-MAS spectra; Figures S6–S12: 1H and ^{13}C , and ^{13}C CP-MAS NMR spectra; Figures S13–S15: Thermogravimetric curves.

Author Contributions: Conceptualization, funding acquisition, project administration, supervision, V.V.; investigation, formal analysis, writing—original draft preparation, M.M., B.P., I.K., D.M., J.P.V. and V.V. visualization, M.C. and I.K., writing—review and editing, B.P., M.C. and V.V. All authors have read and agreed to the published version of the manuscript.

Funding: This work has been fully supported by Croatian Science Foundation under the project (IP-2016-06-4221).

Institutional Review Board Statement: Not applicable.

Informed Consent Statement: Not applicable.

Data Availability Statement: Crystallographic data sets for the structures $[1H]Cl \cdot MeOH$, $[1H]Br$, $[1H](ClA)_{0.5} \cdot 2MeOH$, $[1H]Cl \cdot 0.5VA$, $[1H]Br \cdot 0.5VA$, **2Cl**·MeOH, **2Cl**, **2Br**·0.5MeCN, **1** and **2** are available through the Cambridge Structural Database with deposition numbers CCDC 2155887-2155896. These data can be obtained free of charge via <https://www.ccdc.cam.ac.uk/conts/retrieving.html> (accessed on 2 March 2022) (or from the CCDC, 12 Union Road, Cambridge CB2 1EZ, UK; Fax: +44 1223 336033; E-mail: deposit@ccdc.cam.ac.uk) (accessed on 2 March 2022).

Acknowledgments: We acknowledge the support of project CluK co-financed by the Croatian Government and the European Union through the European Regional Development Fund-Competitiveness and Cohesion Operational Programme (Grant KK.01.1.1.02.0016.). The work of doctoral student Mirna Mandarić has been supported by the “Young researchers’ career development project—training of doctoral students” of the Croatian Science Foundation funded by the European Union from the European Social Fund.

Conflicts of Interest: The authors declare no conflict of interest.

References

1. Su, X.; Aprahamian, I. Hydrazone-based switches, metallo-assemblies and sensors. *Chem. Soc. Rev.* **2014**, *43*, 1963–1981. [[CrossRef](#)] [[PubMed](#)]
2. Lehn, J.-M. From supramolecular chemistry towards constitutional dynamic chemistry and adaptive chemistry. *Chem. Soc. Rev.* **2007**, *36*, 151–160. [[CrossRef](#)] [[PubMed](#)]
3. Banerjee, S.; Ray, A.; Sen, S.; Mitra, S.; Hughes, D.L.; Butcher, R.J.; Batten, S.; Turner, D. Pseudohalide-induced structural variations in hydrazone-based metal complexes: Syntheses, electrochemical studies and structural aspects. *Inorg. Chim. Acta* **2008**, *361*, 2692–2700. [[CrossRef](#)]
4. Jayanthi, E.; Kalaiselvi, S.; Padma, V.V.; Bhuvanesh, N.S.P.; Dharmaraj, N. Solvent assisted formation of ruthenium(III) and ruthenium(II) hydrazone complexes in one-pot with potential in vitro cytotoxicity and enhanced LDH, NO and ROS release. *Dalton Trans.* **2016**, *45*, 1693–1707. [[CrossRef](#)]
5. Li, Y.; Yang, Z.; Zhou, M.; Li, Y.; He, J.; Wang, X.; Lin, Z. Ni(II) and Co(II) complexes of an asymmetrical aroylhydrazone: Synthesis, molecular structures, DNA binding, protein interaction, radical scavenging and cytotoxic activity. *RSC Adv.* **2017**, *7*, 41527–41539. [[CrossRef](#)]
6. Ay, B.; Şahin, O.; Demir, B.S.; Saygideger, Y.; López-De-Luzuriaga, J.M.; Mahmoudi, G.; Safin, D.A. Antitumor effects of novel nickel–hydrazone complexes in lung cancer cells. *New J. Chem.* **2020**, *44*, 9064–9072. [[CrossRef](#)]
7. Kobayashi, A.; Yamamoto, D.; Horiki, H.; Sawaguchi, K.; Matsumoto, T.; Nakajima, K.; Chang, H.-C.; Kato, M. Photoinduced Dimerization Reaction Coupled with Oxygenation of a Platinum(II)–Hydrazone Complex. *Inorg. Chem.* **2014**, *53*, 2573–2581. [[CrossRef](#)]
8. Bebić, N.; Topić, E.; Mandarić, M.; Hrenar, T.; Vrdoljak, V. Extending the structural landscape of Mo(VI) hydrazonato inorganic–organic POM-hybrids: An experimental and computational study. *CrystEngComm* **2021**, *23*, 6349–6358. [[CrossRef](#)]
9. Vrdoljak, V.; Prugovečki, B.; Matković-Čalogović, D.; Dreos, R.; Siega, P.; Tavagnacco, C. Zigzag Chain, Square Tetranuclear, and Polyoxometalate-Based Inorganic–Organic Hybrid Compounds—Molybdenum vs. Tungsten. *Cryst. Growth Des.* **2010**, *10*, 1373–1382. [[CrossRef](#)]
10. Vrdoljak, V.; Prugovečki, B.; Matković-Čalogović, D.; Pisk, J.; Dreos, R.; Siega, P. Supramolecular Hexagon and Chain Coordination Polymer Containing the MoO₂²⁺ Core: Structural Transformation in the Solid State. *Cryst. Growth Des.* **2011**, *11*, 1244–1252. [[CrossRef](#)]
11. Vrdoljak, V.; Prugovečki, B.; Matković-Čalogović, D.; Hrenar, T.; Dreos, R.; Siega, P. Three Polymorphic Forms of a Monomeric Mo(VI) Complex: Building Blocks for Two Metal–Organic Supramolecular Isomers. Intermolecular Interactions and Ligand Substituent Effects. *Cryst. Growth Des.* **2013**, *13*, 3773–3784. [[CrossRef](#)]
12. Maurya, M.R.; Rana, L.; Avecilla, F. Catalytic oxidation of internal and terminal alkenes by oxidoperoxido-molybdenum(VI) and dioxido-molybdenum(VI) complexes. *Inorg. Chim. Acta* **2015**, *429*, 138–147. [[CrossRef](#)]
13. Sinha, S.; Chakraborty, M.; Pramanik, N.R.; Raychaudhuri, T.K.; Mondal, T.K.; Sarkar, D.; Drew, M.G.; Ghosh, S.; Mandal, S.S. Dimer formation by symbiotic donor–acceptor interaction between two molecules of a specially designed dioxomolybdenum(VI) complex containing both donor and acceptor centers—A structural, spectroscopic and DFT study. *Polyhedron* **2013**, *55*, 192–200. [[CrossRef](#)]
14. Bafti, A.; Razum, M.; Topić, E.; Agustin, D.; Pisk, J.; Vrdoljak, V. Implication of oxidant activation on olefin epoxidation catalysed by Molybdenum catalysts with aroylhydrazonato ligands: Experimental and theoretical studies. *Mol. Catal.* **2021**, *512*, 111764. [[CrossRef](#)]
15. Mihalinc, J.; Pajski, M.; Guillo, P.; Mandarić, M.; Bebić, N.; Pisk, J.; Vrdoljak, V. Alcohol Oxidation Assisted by Molybdenum Hydrazonato Catalysts Employing Hydroperoxide Oxidants. *Catalysts* **2021**, *11*, 881. [[CrossRef](#)]
16. Pisk, J.; Agustin, D.; Vrdoljak, V. Tetranuclear molybdenum(VI) hydrazonato epoxidation (pre)catalysts: Is water always the best choice? *Catal. Commun.* **2020**, *142*, 106027. [[CrossRef](#)]
17. Biswal, D.; Pramanik, N.R.; Chakrabarti, S.; Drew, M.G.B.; Sarkar, B.; Maurya, M.R.; Mukherjee, S.K.; Chowdhury, P. New polymeric, dimeric and mononuclear dioxido-molybdenum(VI) complexes with an ONO donor ligand: Crystal structures, DFT calculations, catalytic performance and protein binding study of the ligand. *New J. Chem.* **2017**, *41*, 4116–4137. [[CrossRef](#)]
18. Kargar, H.; Fallah-Mehrjardi, M.; Behjatmanesh-Ardakani, R.; Munawar, K.S.; Ashfaq, M.; Tahir, M.N. Selective oxidation of benzyl alcohols to benzaldehydes catalyzed by dioxomolybdenum Schiff base complex: Synthesis, spectral characterization, crystal structure, theoretical and computational studies. *Transit. Met. Chem.* **2021**, *46*, 437–455. [[CrossRef](#)]
19. Kargar, H.; Fallah-Mehrjardi, M.; Behjatmanesh-Ardakani, R.; Munawar, K.S.; Ashfaq, M.; Tahir, M.N. Synthesis, spectral characterization, SC-XRD, HSA, DFT and catalytic activity of a dioxido-molybdenum complex with aminosalicyl-hydrazone Schiff base ligand: An experimental and theoretical approach. *Polyhedron* **2021**, *208*, 115428. [[CrossRef](#)]
20. Cvijanović, D.; Pisk, J.; Pavlović, G.; Šišak-Jung, D.; Matković-Čalogović, D.; Cindrić, M.; Agustin, D.; Vrdoljak, V. Discrete mononuclear and dinuclear compounds containing a MoO₂²⁺ core and 4-aminobenzhydrazone ligands: Synthesis, structure and organic-solvent-free epoxidation activity. *New J. Chem.* **2019**, *43*, 1791–1802. [[CrossRef](#)]
21. Mazur, L.; Materek, I.; Bond, A.D.; Jones, W. Multicomponent Crystal Forms of a Biologically Active Hydrazone with Some Dicarboxylic Acids: Salts or Cocrystals? *Cryst. Growth Des.* **2019**, *19*, 2663–2678. [[CrossRef](#)]
22. Zhuo, C.; Sun, Y.; Wang, F.; Zhang, J. In Situ Encapsulation of Organic Sulfates in Layered Structures of Zinc and Tris(4-(1H-Imidazol-1-yl)phenyl)amine. *Cryst. Growth Des.* **2020**, *20*, 4228–4231. [[CrossRef](#)]

23. Braga, D.; Grepioni, F.; Shemchuk, O. Organic–inorganic ionic co-crystals: A new class of multipurpose compounds. *CrystEngComm* **2018**, *20*, 2212–2220. [[CrossRef](#)]
24. Ngan, N.K.; Wong, R.C.S.; Lo, K.M.; Ng, S.W. [N'-(5-Chloro-2-oxidobenzyl-κO)-2,4-dihydroxybenzohydrazidato-κ2N',O](methanol-κO)dioxidomolybdenum(VI)-4,4'-bipyridine (1/1). *Acta Crystallogr. Sect. E Struct. Rep. Online* **2011**, *67*, m747. [[CrossRef](#)] [[PubMed](#)]
25. Liu, H.X.; Zhang, X.M.; Wang, X. Synthesis, characterization and crystal structure of cis-dioxomolybdenum (VI)-Schiff base complex [MoO₂(O-C₆H₄CH=NN-COCH₂NC₅H₅)CH₃OH]Cl. *Polyhedron* **1994**, *13*, 441–444. [[CrossRef](#)]
26. Vrdoljak, V.; Prugovečki, B.; Pulić, I.; Cigler, M.; Sviben, D.; Vuković, J.P.; Novak, P.; Matković-Čalogović, D.; Cindrić, M. Dioxidomolybdenum(VI) complexes with isoniazid-related hydrazones: Solution-based, mechanochemical and UV-light assisted deprotonation. *New J. Chem.* **2015**, *39*, 7322–7332. [[CrossRef](#)]
27. Mandarić, M.; Prugovečki, B.; Cvijanović, D.; Vuković, J.P.; Lovrić, J.; Skočibušić, M.; Odžak, R.; Cindrić, M.; Vrdoljak, V. Vapour- and solvent-mediated crystalline transformations in Mo(vi) hydrazone complexes controlled by noncovalent interactions. *CrystEngComm* **2019**, *21*, 6281–6292. [[CrossRef](#)]
28. Kabir, K.; Tobita, H.; Matsuo, H.; Nagayoshi, K.; Yamada, K.; Adachi, K.; Sugiyama, Y.; Kitagawa, S.; Kawata, S. Crystal Engineering Using the Versatility of 2,5-Dichloro-3,6-dihydroxy-1,4-benzoquinone with Organic and Metal Complex Partners. *Cryst. Growth Des.* **2003**, *3*, 791–798. [[CrossRef](#)]
29. Molčanov, K.; Kojić-Prodić, B.; Meden, A. Unique Electronic and Structural Properties of 1,4-Benzoquinones: Crystallochemistry of Alkali Chloranilate Hydrates. *Croat. Chem. Acta* **2009**, *82*, 387–396. Available online: <https://hrcak.srce.hr/39656> (accessed on 9 April 2021).
30. Ishida, H. Pyrrolidinium chloranilate. *Acta Crystallogr. Sect. E Struct. Rep. Online* **2004**, *60*, o974–o976. [[CrossRef](#)]
31. Gotoh, K.; Asaji, T.; Ishida, H. Hydrogen bonding in two solid phases of phenazine–chloranilic acid (1/1) determined at 170 and 93 K. *Acta Crystallogr. Sect. C Cryst. Struct. Commun.* **2006**, *63*, o17–o20. [[CrossRef](#)] [[PubMed](#)]
32. Kühn, O.; Goutal, S. Acid/Base versus Redox Reaction—The Case of Chloranilic Acid and Hydrazine: A Supramolecular Decision? *Cryst. Growth Des.* **2005**, *5*, 1875–1879. [[CrossRef](#)]
33. Dworniczak, M. Anion radical formation in the reaction of chloranilic acid with n-methylpiperidine in acetonitrile. *React. Kinet. Catal. Lett.* **2003**, *78*, 65–72. [[CrossRef](#)]
34. Chang, M.; Kobayashi, A.; Nakajima, K.; Chang, H.-C.; Kato, M. Dimensionality Control of Vapochromic Hydrogen-Bonded Proton-Transfer Assemblies Composed of a Bis(hydrazone)iron(II) Complex. *Inorg. Chem.* **2011**, *50*, 8308–8317. [[CrossRef](#)] [[PubMed](#)]
35. Kobayashi, A.; Dosen, M.-A.; Chang, M.; Nakajima, K.; Noro, S.-I.; Kato, M. Synthesis of Metal–Hydrazone Complexes and Vapochromic Behavior of Their Hydrogen-Bonded Proton-Transfer Assemblies. *J. Am. Chem. Soc.* **2010**, *132*, 15286–15298. [[CrossRef](#)]
36. Kawata, S.; Kitagawa, S.; Kumagai, H.; Kudo, C.; Kamesaki, H.; Ishiyama, T.; Suzuki, R.; Kondo, M.; Katada, M. Rational Design of a Novel Intercalation System. Layer-Gap Control of Crystalline Coordination Polymers, [[Cu(CA)(H₂O)_m](G)]_n (m = 2, G = 2,5-Dimethylpyrazine and Phenazine; m = 1, G = 1,2,3,4,6,7,8,9-Octahydrophenazine). *Inorg. Chem.* **1996**, *35*, 4449–4461. [[CrossRef](#)]
37. Jurić, M.; Molčanov, K.; Žilić, D.; Kojić-Prodić, B. From mononuclear to linear one-dimensional coordination species of copper(II)-chloranilate: Design and characterization. *RSC Adv.* **2016**, *6*, 62785–62796. [[CrossRef](#)]
38. Kabir, M.; Miyazaki, N.; Kawata, S.; Adachi, K.; Kumagai, H.; Inoue, K.; Kitagawa, S.; Iijima, K.; Katada, M. Novel layered structures constructed from iron–chloranilate compounds. *Coord. Chem. Rev.* **2000**, *198*, 157–169. [[CrossRef](#)]
39. Maurya, M.R.; Rana, L.; AVECILLA, F. Molybdenum complexes with a μ-O[MoO₂]₂ core: Their synthesis, crystal structure and application as catalysts for the oxidation of bicyclic alcohols using N-based additives. *New J. Chem.* **2017**, *41*, 724–734. [[CrossRef](#)]
40. Gündüz, T. Some New Organic Complexes of Molybdenum. *Commun. Fac. Sci. Univ. Ank. Ser. B Chem. Chem. Eng.* **1964**, *11*, 021–031. [[CrossRef](#)]
41. Gomes, L.R.; Low, J.N.; Correia, N.R.D.L.; Nogueira, T.C.; Pinheiro, A.C.; de Souza, M.V.; Wardell, J.L.; Wardell, S.M. Crystal structures and Hirshfeld surface analysis of four 1,4-bis(methoxyphenyl)-2,3-diazabuta-1,3-dienes: Comparisons of the intermolecular interactions in related compounds. *Z. Krist. Cryst. Mater.* **2019**, *234*, 59–71. [[CrossRef](#)]
42. Ghosh, M.; Ta, S.; Matalobos, J.S.; Das, D. Azine based smart probe for optical recognition and enrichment of Mo(VI). *Dalton Trans.* **2018**, *47*, 11084–11090. [[CrossRef](#)] [[PubMed](#)]
43. Chen, G.J.J.; McDonald, J.W.; Newton, W.E. Synthesis of molybdenum(IV) and molybdenum(V) complexes using oxo abstraction by phosphines. Mechanistic implications. *Inorg. Chem.* **1976**, *15*, 2612–2615. [[CrossRef](#)]
44. Arnáiz, F.J.; Aguado, R.; Pedrosa, M.R.; Mahía, J.; Maestro, M.A. Addition compounds of MoO₂Br₂ from MoO₂Br₂(H₂O)₂. Molecular structure of MoO₂Br₂[OP[N(CH₃)₂]₃]₂ and MoO₂Br₂[CH₂[P(O)(C₆H₅)₂]₂]. *Polyhedron* **2002**, *21*, 1635–1642. [[CrossRef](#)]
45. Graham, R.L.; Hepler, L.G. Heats of Formation of Molybdenum Oxychlorides. *J. Phys. Chem.* **1959**, *63*, 723–724. [[CrossRef](#)]
46. Pisk, J.; Hrenar, T.; Rubčić, M.; Pavlović, G.; Damjanović, V.; Lovrić, J.; Cindrić, M.; Vrdoljak, V. Comparative studies on conventional and solvent-free synthesis toward hydrazones: Application of PXRD and chemometric data analysis in mechanochemical reaction monitoring. *CrystEngComm* **2018**, *20*, 1804–1817. [[CrossRef](#)]
47. Kurteva, V.B.; Simeonov, S.; Stoilova-Disheva, M. Symmetrical Acyclic Aryl Aldazines with Antibacterial and Antifungal Activity. *Pharmacol. Pharm.* **2011**, *2*, 1. [[CrossRef](#)]

48. *CrysAlisPro Software System, Version 1.171.38.41*; Rigaku Oxford Diffraction: Oxford, UK, 2015.
49. Farrugia, L.J. WinGX and ORTEP for Windows: An update. *J. Appl. Crystallogr.* **2012**, *45*, 849–854. [[CrossRef](#)]
50. Sheldrick, G.M. A short history of SHELX. *Acta Crystallogr. Sect. A* **2008**, *64*, 112–122. [[CrossRef](#)]
51. Sheldrick, G.M. Crystal structure refinement with SHELXL. *Acta Crystallogr. Sect. C Struct. Chem.* **2015**, *71*, 3–8. [[CrossRef](#)]
52. Spek, A.L. Structure validation in chemical crystallography. *Acta Crystallogr. Sect. D Biol. Crystallogr.* **2009**, *65*, 148–155. [[CrossRef](#)]
53. Macrae, C.F.; Bruno, I.; Chisholm, J.A.; Edgington, P.R.; McCabe, P.; Pidcock, E.; Rodriguez-Monge, L.; Taylor, R.J.; van de Streek, J.; Wood, P. Mercury CSD 2.0—New features for the visualization and investigation of crystal structures. *J. Appl. Crystallogr.* **2008**, *41*, 466–470. [[CrossRef](#)]
54. Degen, T.; Sadki, M.; Bron, E.; König, U.; Nénert, G. The High Score suite. *Powder Diffr.* **2014**, *29*, S13–S18. [[CrossRef](#)]
55. Mosmann, T. Rapid colorimetric assay for cellular growth and survival: Application to proliferation and cytotoxicity assays. *J. Immunol. Methods* **1983**, *65*, 55–63. [[CrossRef](#)]
56. Lei, Y.; Fu, C. Synthesis and X-Ray Structural Characterization of Dioxomolybdenum(VI) Complexes with 2'-(5-Chloro-2-hydroxybenzylidene)isonicotinohydrazide and 2'-(2-Hydroxy-3-methoxybenzylidene)isonicotinohydrazide. *Synth. React. Inorg. Met. Nano-Metal Chem.* **2011**, *41*, 704–709. [[CrossRef](#)]
57. Alghool, S.; Slebodnick, C. Supramolecular structures of mononuclear and dinuclear dioxomolybdenum(VI) complexes via hydrogen bonds and π - π stacking, thermal studies and electrochemical measurements. *Polyhedron* **2014**, *67*, 11–18. [[CrossRef](#)]
58. Bikas, R.; Lippolis, V.; Noshiranzadeh, N.; Farzaneh-Bonab, H.; Blake, A.J.; Siczek, M.; Hosseini-Monfared, H.; Lis, T. Electronic Effects of Aromatic Rings on the Catalytic Activity of Dioxidomolybdenum(VI)–Hydrazone Complexes. *Eur. J. Inorg. Chem.* **2016**, *2017*, 999–1006. [[CrossRef](#)]
59. Randell, N.M.; Thompson, L.K.; Dawe, L.N. 6,6'-Dimethoxy-2,2'-[*(E,E)*-hydrazine-1,2-diylidene]bis(methanylylidene)diphenol methanol disolvate. *Acta Crystallogr. Sect. E Struct. Rep. Online* **2012**, *68*, o2711. [[CrossRef](#)] [[PubMed](#)]